http://www.jstage.jst.go.jp/browse/biophysics

BIOPHYSICS

Vol. 2, pp. 45–56 (2006)
doi: 10.2142/biophysics.2.45

Roles of charged residues in pH-dependent redox properties of cytochrome c_3 from *Desulfovibrio vulgaris* Miyazaki F

Naoki Yahata[1], Kiyoshi Ozawa[2,5], Yusuke Tomimoto[3], Kumiko Morita[3], Hirofumi Komori[3,4], Hideaki Ogata[3], Yoshiki Higuchi[3,4] and Hideo Akutsu[1]

[1]*Institute for Protein Research, Osaka University, Yamadaoka, Suita 565-0871, Japan*
[2]*Faculty of Engineering, Yokohama National University, Hodogaya-ku, Yokohama 240-8501, Japan*
[3]*Graduate School of Life Science, University of Hyogo and Himeji Institute of Technology, Koto, Kamigori, Hyogo 678-1297, Japan*
[4]*RIKEN SPring-8 Center, 1-1-1 Koto, Sayo-cho, Sayo-gun, Hyogo 679-5148, Japan*
[5]*Present address: Research School of Chemistry, Australian National University, Canberra, ACT 0200, Australia*

Received 24 March, 2006; accepted 26 May, 2006

Complicated pH-properties of the tetraheme cytochrome c_3 (cyt c_3) from *Desulfovibrio vulgaris* Miyazaki F (*Dv*MF) were examined by the pH titrations of ^{1}H-^{15}N HSQC spectra in the ferric and ferrous states. The redox-linked pK_a shift for the propionate group at C13 of heme 1 was observed as the changes of the NH signals around it. This pK_a shift is consistent with the redox-linked conformational alteration responsible for the cooperative reduction between hemes 1 and 2. On the other hand, large chemical shift changes caused by the protonation/deprotonation of Glu41 and/or Asp42, and His67 were redox-independent. Nevertheless, these charged residues affect the redox properties of the four hemes. Furthermore, one of interesting charged residues, Glu41, was studied by site-directed mutagenesis. E41K mutation increased the microscopic redox potentials of heme 1 by 46 and 34 mV, and heme 2 by 35 and 30 mV at the first and last reduction steps, respectively. Although global folding in the crystal structure of E41K cyt c_3 is similar to that of wild type, local change was observed in ^{1}H NMR spectrum. Glu41 is important to keep the stable conformation in the region between hemes 1 and 2, controlling the redox properties of *Dv*MF cyt c_3. In contrast, the kinetic parameters for electron transfer from *Dv*MF [NiFe] hydrogenase were not influenced by E41K mutation. This suggests that the region between hemes 1 and 2 is not involved in the interaction with [NiFe] hydrogenase, and it supports the idea that heme 4 is the exclusive entrance gate to accept the electron in the initial reduction stage.

Key words: tetraheme protein, nuclear magnetic resonance (NMR), site-directed mutagenesis, electron transfer, hydrogenase

Abbreviations: HSQC, heteronuclear single-quantum coherence; TOCSY, total correlation spectroscopy; NOESY, nuclear Overhauser effect spectroscopy; HEPES, *N*-2-Hydroxyethylpiperazine-*N*′-2-ethanesulfonic acid.

Corresponding author: Hideo Akutsu, Institute for Protein Research, Osaka University, Yamadaoka, Suita 565-0871, Japan.
e-mail: akutsu@protein.osaka-u.ac.jp

The oxidation-reduction (redox) potential is an important factor in the electron transfer reaction[1]. The redox potential of the metal center in a protein is regulated by various factors. They are especially complicated in a protein possessing multi-redox centers. Cytochrome c_3 (cyt c_3) is a small soluble protein (M_r~14000) including four *c*-type hemes. The unique feature of cyt c_3 is its very low redox potentials (about −300 mV in average), which is considered to be important for sulfate respiration in sulfate-reducing bacteria. The microscopic redox potentials of individual hemes and the interacting potentials between two hemes were determined for the cyt c_3 from *Desulfovibrio vulgaris* Miyazaki F (*Dv*MF)[2,3], *D. vulgaris* Hildenborough (*Dv*H)[4,5],

D. desulfuricans ATCC 27774 (*Dd*A)[6], and *D. gigas* (*Dg*)[7,8] in different ways. These cyt c_3 were categorized as the 2-4-2-4 group, which has heme binding motifs CXXCH, CXXXXCH, CXXCH, and CXXXXCH (X is any amino acid) along the sequence[9]. Although they revealed highly homologous three-dimensional (3D) structures, redox properties are different. This diversity is considered to be attributed to the relatively low sequence homology.

The heme methyl chemical shifts of cyt c_3 from *Dv*MF showed complicated pH dependences in a variety of redox states[3]. Some ionizable groups including charged residues were assumed to be responsible for these properties around neutral pH range. It was suggested that propionate group at C13 of heme 1 was responsible for the redox potential change of heme 1 in the acidic pH region[3]. The importance of this propionate group was also suggested in three other cyt c_3 (*Dv*H, *Dd*A, and *Dg*). The roles of more ionizable groups were examined and discussed by the structural analyses[10 and references therein], the site-directed mutagenesis[11], and the theoretical methods[12–16], but they could not explain the complicated pH dependence of cyt c_3 from *Dv*MF. Recently, the NMR resonance assignments of the NH groups for ferric and ferrous cyt c_3 from *Dv*MF were established[17,18]. For the first time, we have examined the complicated pH-properties of ferric and ferrous cyt c_3 in the amino acid level.

The experiments mentioned above indicated that Glu41 located between hemes 1 and 2 was an interesting target in terms of pH-dependent properties of *Dv*MF cyt c_3. The $O^{\varepsilon 1}$ atom of Glu41 forms hydrogen bond with the OH group of Tyr43 in the oxidized crystal structure[19]. It was suggested that the conformational alteration of aromatic ring of Tyr43 is involved in the cooperative reduction between hemes 1 and 2[17]. Actually, replacement of Tyr43 by leucine induced the increase of the redox potential for heme 1 and the decrease of the cooperativity between hemes 1 and 2[9,20]. In the 2-4-2-4 group, these two residues are conserved as Glu or Gln, and Tyr or Phe, respectively[9]. Although this hydrogen bond is not essential to control the redox properties as previously reported[20], the proximity of Glu41 to Tyr43 might affect the redox properties of the *Dv*MF cyt c_3.

It was shown that several charged residues around heme 4 are important to form the transient complex with electron exchange partners[18 and references therein]. Additionally, it was suggested that the regions around other hemes may be also involved in the interaction with type II cyt c_3[21,22] and [NiFe] hydrogenase[18,23]. Therefore, Glu41 located between hemes 1 and 2 could affect the interaction with [NiFe] hydrogenase as well.

To elucidate the structural and functional roles of Glu41, it was replaced by lysine and glutamine in this work. As references, K101M and K104M mutants were also examined. Lys101 and Lys104 are close to heme 4 and heme 3, respectively. Furthermore, the kinetic property of E41K on the reduction by [NiFe] hydrogenase was examined. Results obtained from these studies are discussed on the basis of the crystal structures of the E41K and E41Q cyt c_3 together with previously reported results.

Materials and methods

Site-directed mutagenesis and purification

All mutations were introduced into the pKFC3k plasmid, which contains the *Dv*MF cyt c_3 gene[20]. Site-directed mutagenesis was conducted with a Mutan-Super Express Km kit (Takara Bio, Inc., Japan). Synthetic oligonucleotides for E41K (5′-GTCAACGGCAAGAAAGACTACCAGAAGTG-3′), E41Q (5′-GTCAACGGCAAGCAAGACTACCAGAA GTG-3′), and K104M (5′-TGCAAGGGCTCCATGTGCCA TAGCTAG-3′) were purchased from Invitrogen Co., Japan. The mutations were confirmed by nucleotide sequencing. This was performed with an ABI PRISM 310 genetic analyzer (Applied Biosystems Japan Ltd.) using a DNA sequence kit, BigDye Terminator Cycle Sequencing Ready Reaction (Applied Biosystems Japan Ltd.), and two M13 primers, RV-N and M4 (Takara Bio, Inc., Japan). K101M plasmid was obtained as mentioned previously[18]. Wild-type and mutated cyt c_3 genes were overexpressed in *Shewanella oneidensis* TSP-C and purified as described previously[18,24].

NMR measurements

^{15}N-labeled cyt c_3 were obtained as mentioned previously[18]. ^{1}H-^{15}N HSQC spectra were recorded with AVANCE DRX-500 NMR spectrometers (Bruker, Germany) at 303 K. The data size was 2048 (^{1}H)×128 (^{15}N). The spectral widths were 21 (^{1}H)×40 (^{15}N) ppm for the oxidized sample and 18 (^{1}H)×38 (^{15}N) ppm for the reduced one. NMR samples were prepared as previously described[25]. Additionally, 30 mM sodium phosphate (NaP_i) and sodium borate buffers were used for pH 5.2–7.8 and pH 8.5–9.0, respectively.

All ^{1}H NMR spectra were recorded with AVANCE DRX-400, DRX-600 and DRX-800 NMR spectrometers (Bruker, Germany). NMR samples were prepared as previously described[25]. For the one-dimensional (1D) ^{1}H NMR experiments, the protein concentration was 1 mM in either 30 or 100 mM NaP_i buffer at p^{2}H 7.0. TOCSY spectra (mixing time, 60 ms) and NOESY spectra (mixing time, 50 and 400 ms) were obtained for cyt c_3 mutants in the reduced state to assign each heme, as reported previously[26]. Chemical exchange spectra with the mixing time of 15 ms, the data size of 2048×512, and the spectrum width of 24 kHz, were recorded for different intermediate oxidation stages to determine the chemical shifts in the five oxidation states. The reduction fractions of each heme were determined from the heme methyl chemical shifts in the five macroscopic oxidation states[2,9]. p^{2}H titrations of chemical exchange spectra were performed in the same condition. p^{2}H was adjusted by adding ^{2}HCl and/or NaO^2H. The chemical shifts of the heme methyl groups in the fully oxidized (S_0), one-electron-reduced (S_1), two-electron-reduced (S_2), and three-electron-reduced (S_3) were assigned based on the chemical shifts in

the fully reduced state (S_4) at p^{2}H 7.0[26]. Chemical shifts are presented in parts per million (ppm) relative to the internal standard, 2,2-dimethyl-2-silapentane-5-sulfonate (DSS).

Determination of macroscopic redox potentials

Redox potentials of the wild-type and mutated cyt c_3 were measured by differential pulse polarography. The polarograms were obtained at 30°C with a 394 Digital Electrochemical Trace Analysis System (PerkinElmer, Inc.), which was controlled with Model 394 Analytical Voltammetry Software. The working electrode was a dropping mercury electrode, with a platinum wire coil as the counter electrode and an Ag/AgCl electrode as the reference electrode. Pulse height, scan rate, and drop time were 20 mV, 2 mV s^{-1}, and 2 s, respectively. Cyt c_3 was dissolved in NaP_i buffer at pH 7.0 (final approximately 100 μM). Buffer concentration was identical to the NMR sample. The polarograms were fitted using the analytical equation for the four consecutive one-electron reversible electrode reactions[27]. Macroscopic redox potentials are referred to the standard hydrogen electrode (SHE).

Measurement of cytochrome c_3 reduction by [NiFe] hydrogenase

Anaerobic cuvettes were filled with various concentrations (final 1–30 μM) of the protein and 50 mM HEPES (pH 7.0). They were bubbled with high-grade hydrogen gas for 30 min. The change of the absorbance at 552 nm ($\delta\varepsilon_{552}$= $\varepsilon_{552red}-\varepsilon_{552ox}$=84000 M^{-1} cm^{-1}) was measured after the addition of hydrogenase (final 7 nM). The slope of the tangent drawn at the beginning of the recorded trace was used to calculate the initial reduction rate of cyt c_3, which was collected using the hydrogenase activity. The hydrogenase activity was determined according to previously reported method[18]. K_m and k_{cat} were obtained by nonlinear least-squares fitting of the Michaelis–Menten equation to the observed data.

Crystallization and structure determination

Crystals of E41K cyt c_3 from *Dv*MF were grown at 10°C according to the previously reported procedure[20]. In the crystallization of E41Q, 2-methyl-2,4-pentandiol (MPD) was used as a precipitant (an ethanol substitute). Diffraction experiments were carried out at 100 K using synchrotron X-ray beams (wavelengths: 0.700 Å, E41K; and 1.000 Å, E41Q) at the BL44B2 beam line of SPring-8. The crystals of E41K and E41Q belong to orthorhombic space group $P2_12_12_1$. Diffraction data of E41K and E41Q were processed and merged with the programs of MOSFILM[28] and SCALA[29], respectively. The structure refinement was done by the program CNS[30] using the atomic coordinates of the wild-type cyt c_3 at 1.8 Å resolution[19]. In the case of E41K, the structure was further refined by the program SHELXL[31] with anisotropic B-factor refinement for all atoms. At the final stage, hydrogen atoms were incorporated at the calculated positions for E41K.

Results

pH titrations of ^{1}H-^{15}N HSQC spectra

The pH titrations of ^{1}H-^{15}N HSQC spectra for the ferric and ferrous cyt c_3 were performed in the pH range of 5.2–9.0. The superposition of the HSQC spectra in the oxidized state acquired at various pH values are shown in Figure 1A. Several signals indicated distinct transitions either in the

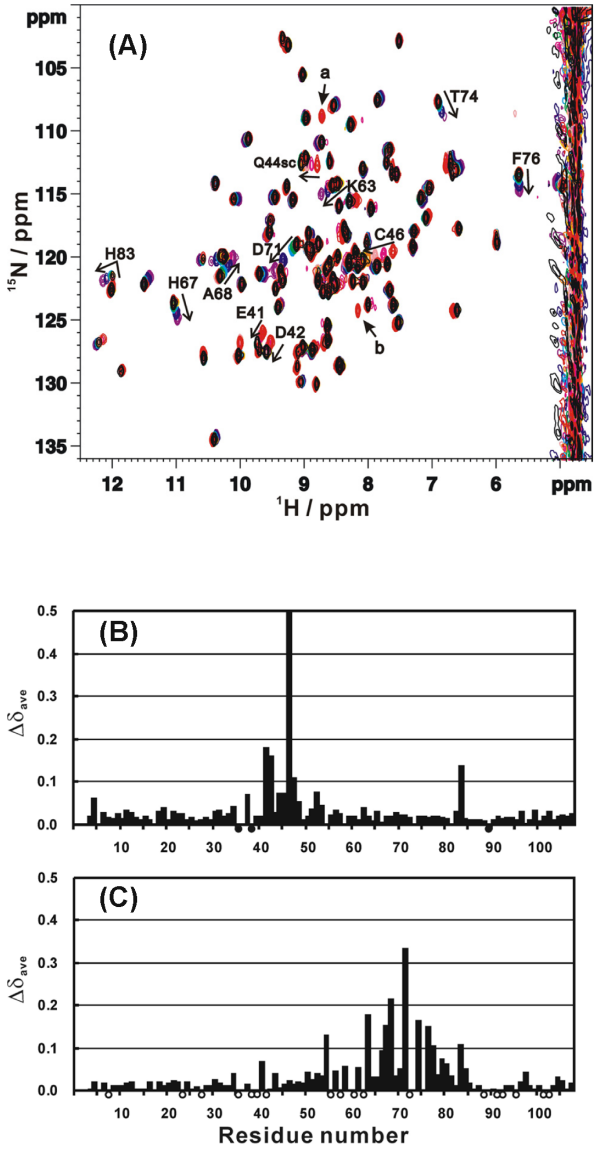

Figure 1 (A) Superposition of ^{1}H-^{15}N HSQC spectra of ferric cytochrome c_3 at various pH values from pH 5.2 (red) through 7.0 (black) to 9.0 (purple). The direction of an arrow indicates the increase of pH value. (B, C) Average chemical shift differences ($\Delta\delta_{ave}$) between pH 5.2 and 7.0, and pH 7.0 and 8.5, respectively. Filled circles indicate the residues whose NH signals were assigned at pH 6.0 although not assigned at pH 7.0[18]. Open circles indicate the residues whose NH signals were not detected at pH 8.5 although assigned at pH 7.0.

acidic or basic pH region. In a pH range lower than 6, two non-assigned signals, named "a" (^{1}H, 8.72 ppm; ^{15}N, 109.1 ppm) and "b" (8.15; 124.5) are observed (Fig. 1A). These signals could be ascribed to non-assigned backbone amides, Ala1 and Gly73. The NH signal of Gly73 in the reduced cyt c_3 was assigned (^{1}H, 8.92 ppm; ^{15}N, 109.6 ppm)[17]. Signal "a" can be ascribed to Gly73 based on the assignment in the reduced state and the averaged ^{15}N amide chemical shift data of each amino acid residue[32]. The appearance of Ala1 amide signal clearly indicates the presence of another alanine residue at the N-terminus as previously reported[33]. To estimate the effects of the pH changes on the properties of cyt c_3, the average chemical shift differences ($\Delta\delta_{ave}$) of each backbone amide between pH 5.2 and 7.0, and pH 7.0 and 8.5, were calculated using the equation, $\Delta\delta_{ave}=[\Delta\delta H^2+(\Delta\delta N/5)^2]^{1/2}$, where $\Delta\delta$H and $\Delta\delta$N stand for the differences in the ^{1}H and ^{15}N chemical shifts, respectively (Figs. 1B and 1C). The residues whose NH signals indicated larger differences ($\Delta\delta_{ave}\geq0.15$) in the acidic pH region were Glu41, Asp42, Gln44 (side chain NH), and Cys46. In the basic pH region, on the other hand, Lys63, His67, Ala68, Asp71, Thr74, and Phe76 indicated larger differences ($\Delta\delta_{ave}\geq0.15$). These residues were mapped on the crystal structure (Fig. 3A). Additionally, the NH signal of His83 indicated strange transition (Fig. 1A).

On the other hand, the spectra became more complicated in the reduced state compared to those of the oxidized one. In lower pH range than 6.5, many signals derived from the three-electron-reduced state (S_3) and/or two-electron reduced state (S_2) appeared in the spectra because of the shift of the redox-equilibrium between cyt c_3 and hydrogenase. Therefore, the superposition of the HSQC spectra in the reduced state at the pH range from 6.5 to 9.0 is shown in Figure 2A. Furthermore, the average chemical shift differences ($\Delta\delta_{ave}$) of each backbone amide between pH 7.0 and 8.5 were shown in Figure 2B. The residues whose NH signals indicate larger differences ($\Delta\delta_{ave}\geq0.09$) are Leu9, Lys10, Lys45, Cys46, Lys63, Tyr66, His67, Ala68, Asp71, and Phe76. These residues were mapped on the solution structure (Fig. 3B).

The pH titration curves of the amide protons of Glu41 and Asp42 in the oxidized and reduced states are plotted in Figure 4A. For the ferrous cyt c_3, it is assumed that NH signal shifts did not influenced by the redox-equilibrium in the acidic pH region. These titration curves in each redox state are similar, that is, pK_as of these titration curves are not dependent on the redox states. For the residues indicated large NH signal changes in both states, His67, Ala68, Asp71, and Phe76, pH titration curves are also plotted in Figure 4B. These residues also show the similar pH dependences. On the other hand, the titration curves for Leu9, Lys10, Lys45, and Cys46 amide proton signals plotted in Figure 4C revealed different pH dependences between the oxidized and reduced states.

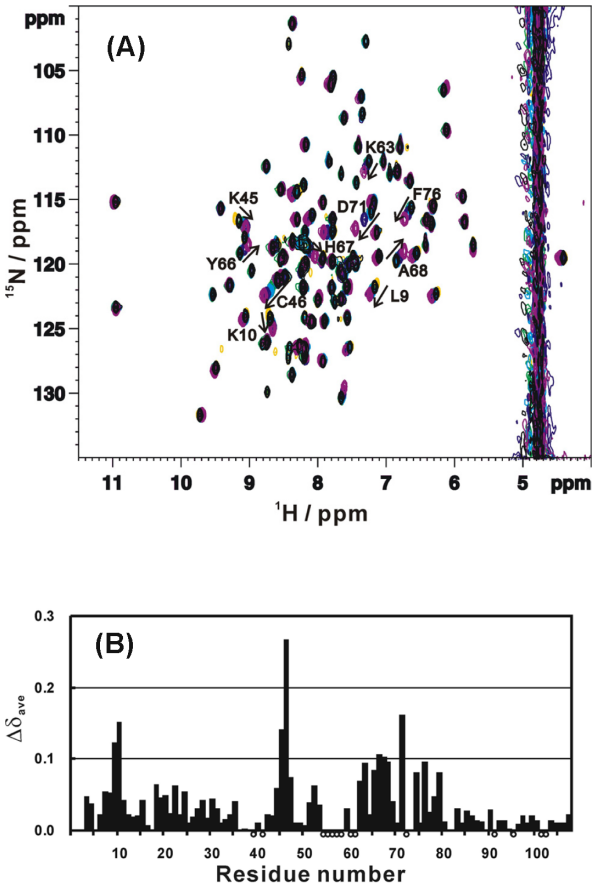

Figure 2 (A) Superposition of ^{1}H-^{15}N HSQC spectra of ferrous cytochrome c_3 at various pH values from pH 6.5 (yellow) through 7.0 (black) to 9.0 (purple). The direction of an arrow indicates the increase of pH value. (B) Average chemical shift differences ($\Delta\delta_{ave}$) between pH 7.0 and 8.5. Open circles indicate the residues whose NH signals were not detected at pH 8.5 although assigned at pH 7.0.

Isolation and characterization of cytochrome c_3 mutants

In light of the results mentioned above, one of two pH-sensitive acidic residues, Glu41 was studied by site-directed mutagenesis. Glu41 was replaced by lysine and glutamine. Additionally, the roles of Lys101 and Lys104 were examined for comparison. Lys101 and Lys104 were replaced by an uncharged residue, methionine. The E41K and K101M cyt c_3 were stably produced and could be purified by previously reported procedure[18]. However, the E41Q and K104M cyt c_3 aggregated in the dialysis after Phenyl-sepharose column. Since these proteins could be dissolved at a relatively high ionic strength, they were applied to SP-sepharose column equilibrated with 30 mM NaP_i buffer containing 40–70 mM NaCl. Finally, the purified E41Q and K104M proteins in 100 mM NaP_i buffer at pH 7.0 could be collected. Thus, these mutants were examined under this condition.

1D ^{1}H NMR spectra were recorded in the oxidized state. To examine the effects of the mutations under the same condition, the spectrum of wild-type cyt c_3 in the 100 mM NaP_i buffer at p^{2}H 7.0 was also recorded. The heme methyl

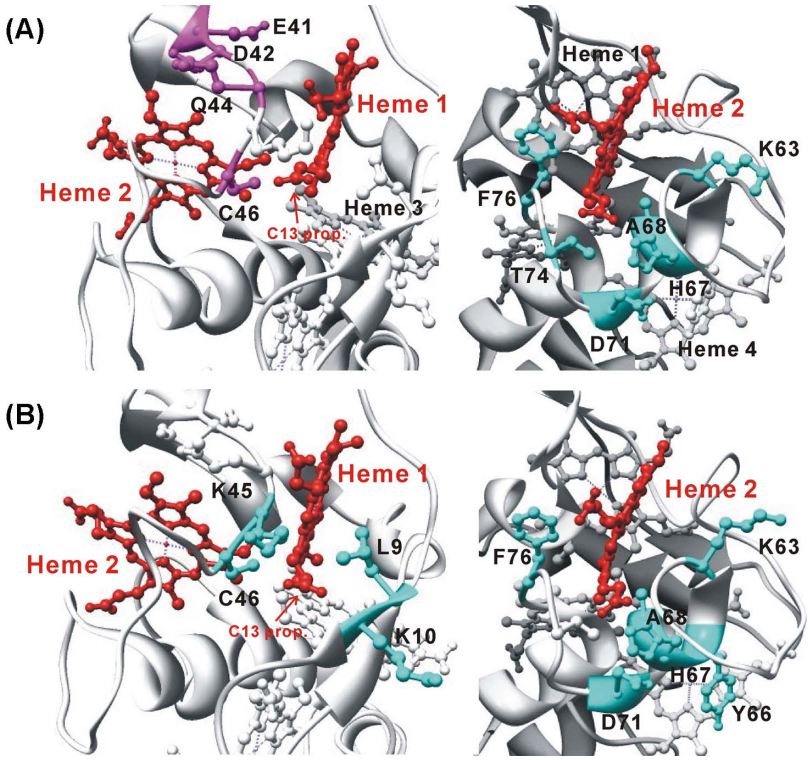

Figure 3 Mappings of the residues showing large pH-dependent shifts on the cytochrome c_3 structures. The regions around heme 1 (left) and heme 2 (right) in the ferric crystal structure (A; PDB code, 1J0O) and the ferrous solution structure (model 1) (B; PDB code, 1IT1). Residues are colored according to the following classification: (A) $\Delta\delta_{ave}$ (pH 5.2–7.0)>0.15 ppm (magenta), $\Delta\delta_{ave}$ (pH 7.0–8.5)>0.15 ppm (cyan); (B) $\Delta\delta_{ave}$ (pH 7.0–8.5)>0.09 ppm (cyan). Focused heme is colored red. These figures were produced with the Chimera program[37].

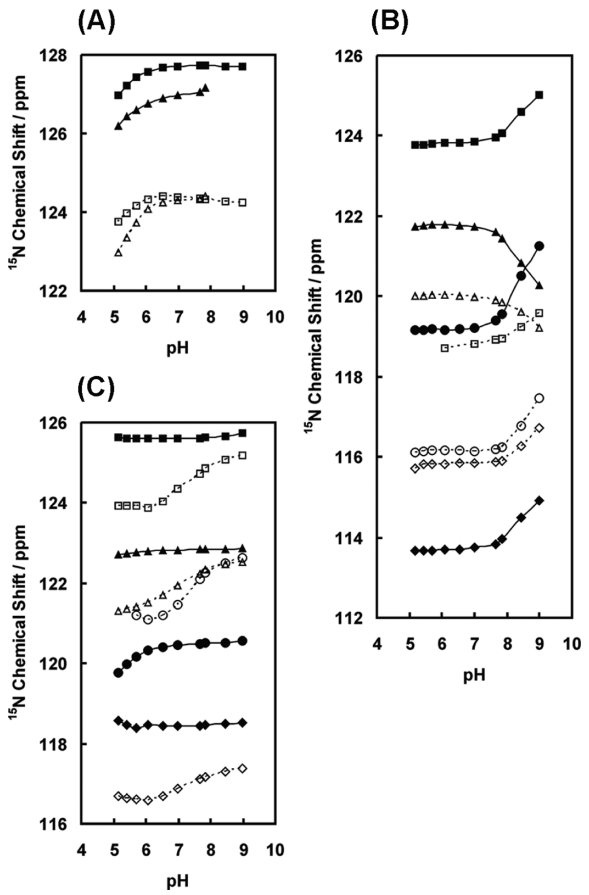

signals in the low magnetic field (13–32 ppm), which are labeled alphabetically (A–J) from low to high magnetic field, were compared. For wild-type cyt c_3, the increase of ionic strength from 30 mM to 100 mM NaP_i did not induce any changes in these signals. The chemical shift assignments of the heme methyl signals of E41K were performed as will be mentioned later. For the E41Q and K104M mutants, only signals A–J were assigned in reference to those observed in E41K and wild type, respectively. The chemical shift differences between the wild type and mutants are summarized in Figure 5. The K101M mutation induced little change in the spectrum as previously reported[18]. The K104M mutation induced a relatively large change for signal E (heme 3), because Lys104 is close to heme 3. In the case of Glu41 mutants, signals for hemes 1 and 2 were mainly affected.

Temperature dependence of 1D ^{1}H NMR spectra in the oxidized state was examined in the range 283–313 K. Generally, line-widths of heme methyl signals gradually broaden according to the decrease of temperature. For the wild-type

Figure 4 pH dependences of ^{15}N chemical shifts of the NH signals for the ferric and ferrous cytochromes c_3. Solid lines (closed signals) and broken ones (open ones) stand for the ferric and ferrous cytochromes c_3, respectively. (A) NH signals for Glu41 and Asp42 stand for triangles and squares, respectively. (B) NH signals for His67, Ala68, Asp71, and Phe76 stand for squares, triangles, circles, and diamonds, respectively. (C) NH signals for Leu9, Lys10, Lys45, and Cys46 stand for triangles, squares, diamonds, and circles, respectively.

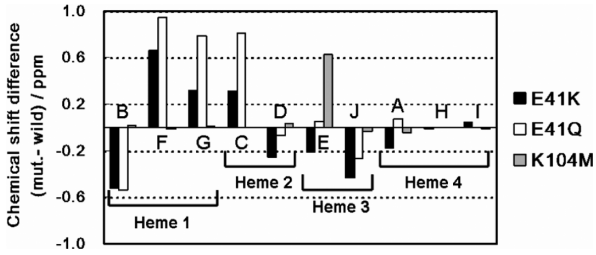

Figure 5 Chemical shift changes in the heme methyl signals of the E41K, E41Q, and K104M ferric cytochromes c_3 in comparison with those of the wild type at p^2H 7.0 and 303 K. E41K, E41Q, and K104M are compared with the wild type in 30, 100, and 100 mM sodium phosphate buffers, respectively. The heme methyl signals which are labeled alphabetically (A–J) from low to high magnetic field were used.

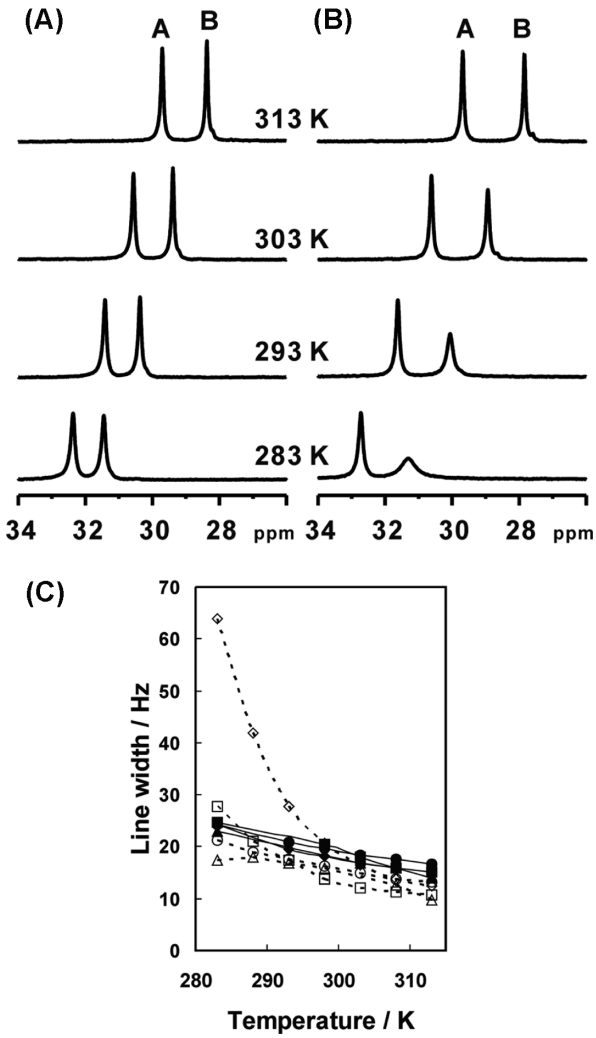

Figure 6 ^1H NMR spectra of wild-type (A) and E41K (B) ferric cytochromes c_3 at a variety of temperatures. Only fingerprint regions are presented. (C) The temperature dependences of line-widths of the heme methyl signals for the wild type and E41K at 600 MHz. Signal B for heme 1, signal C for heme 2, signal E for heme 3, and signal A for heme 4 are represented by diamonds, squares, triangles, and circles, respectively. Solid lines (closed symbols) and broken ones (open ones) stand for the wild type and E41K, respectively.

cyt c_3, the line-width of each heme methyl signal showed the similar tendency in this temperature range (Fig. 6A). The signals for the E41Q, K101M, and K104M mutants revealed similar behavior. For the E41K mutant, however, an obvious change of line-width in the low temperature range was observed (Fig. 6B). Signals B due to heme 1, C due to heme 2, E due to heme 3, and A due to heme 4 of the wild-type and E41K cyt c_3 were fitted to lorentzian using Felix version 2000.1 (Accelrys Software Inc.). Obtained line-widths were plotted as a function of temperature in Figure 6C. The line-width of signal B for E41K cyt c_3 significantly broadened in the low temperature range, which revealed that E41K mutation slowed the exchange rate in a conformational equilibrium around heme 1.

Macroscopic and microscopic redox potentials

The four macroscopic redox potentials of E41K in 30 mM NaP_i buffer (pH 7.0) and wild type, E41Q, and K104M in 100 mM NaP_i buffer (pH 7.0) were determined by theoretical analysis of differential pulse polarography[27]. They are summarized in Table 1. The E41K replacement induced certain changes in the four macroscopic redox potentials, which increased by up to 34 mV. For the E41Q mutant, $E_I°'$, $E_{II}°'$, and $E_{III}°'$ were increased, but the amount of the change was not as large as that of E41K. On the other hand, the K104M mutation induced little change in accordance with the previous report[18].

Following experiments were performed only for E41K and K101M mutants because the obtained results have to be compared with previously reported data under the same buffer condition. 2D chemical exchange spectra of E41K (400 MHz) and K101M (800 MHz) cyt c_3 were obtained for different redox states to determine the chemical shifts of the heme methyl groups in the five macroscopic oxidation states. When the chemical exchange spectra of K101M were recorded at 600 MHz, the heme methyl signals were broadened because of the alteration in the exchange rate and were difficult to be assigned. The spectra recorded at 800 MHz gave narrower line-widths. The assignments of the heme methyl signals in the five macroscopic oxidation states were established on the basis of the chemical shifts in the fully reduced state[26]. The results are summarized in Table 2. It had been shown that the behaviors of signals J and L due to heme 3 during the reduction process were unusual[26]. The behaviors for E41K cyt c_3 were different from those of wild type. The chemical shift of the signal J for S_2 was similar to that for S_1, although that of signal L for S_3 is larger than that for S_2 as in the case of the wild type.

The reduction fraction (R) of each heme (the contribution to total reduction of each heme) can be obtained from the chemical shifts according to the equation, $R_i^j=[\nu(S_{i-1})-\nu(S_i)]/[\nu(S_0)-\nu(S_4)]$, where $\nu(S_i)$ is the chemical shift in oxidation state S_i. The average reduction fractions were calculated under the conditions of $\Sigma_i R_i^j=\Sigma_j R_i^j=1$ (i and j are the heme and reduction step numbers, respectively) using sig-

Table 1 The macroscopic redox potentials of the wild-type and mutated cytochromes c_3 in either 30 mM or 100 mM sodium phosphate buffers at pH 7.0 and 30°C (standard errors of ±2 mV)

	$E_I^{\circ\prime}$	$E_{II}^{\circ\prime}$	$E_{III}^{\circ\prime}$	$E_{IV}^{\circ\prime}$
30 mM				
wild type[a]	−242	−296	−313	−358
E41K	−229 (+13)	−262 (+34)	−290 (+23)	−334 (+24)
K101M[b]	−242 (0)	−293 (+3)	−311 (+2)	−353 (+5)
100 mM				
wild type	−242	−286	−309	−345
E41Q	−230 (+12)	−265 (+21)	−292 (+17)	−342 (+3)
K104M	−244 (−2)	−287 (−1)	−308 (+1)	−347 (−2)

$E_i^{\circ\prime}$ (i=I–IV) is the macroscopic redox potential at the *i*-th reduction step relative to the standard hydrogen electrode (SHE).
[a] From ref. 9.
[b] From ref. 18.

Table 2 Chemical shifts of the heme methyl signals in the five macroscopic oxidation states for E41K and K101M cytochromes c_3 in 30 mM sodium phosphate buffer at p^{2}H 7.0 and 30°C

	Chemical shift in each oxidation state/ppm				
	S_0	S_1	S_2	S_3	S_4
E41K					
Heme 1					
B [18^1-CH_3]	28.79	21.16	9.29	4.46	3.23
F [2^1-CH_3]	19.64	15.11	7.40	3.80	2.78
G [12^1-CH_3]	18.39	13.97	6.27	3.36	2.91
Heme 2					
C [18^1-CH_3]	20.82	19.58	15.23	5.95	3.10
D [7^1-CH_3]	19.98	17.90	13.03	5.41	3.10
Heme 3					
E [12^1-CH_3]	19.69	16.60	15.23	13.39	3.41
J [2^1-CH_3]	13.10	12.23	12.30	11.87	4.64
L [7^1-CH_3]	10.27	8.80	7.36	8.64	3.93
P [18^1-CH_3]	−3.73	−2.26	−1.59	−0.67	3.61
Heme 4					
A [18^1-CH_3]	30.33	19.21	14.35	8.52	3.20
H [2^1-CH_3]	17.52	11.62	9.10	6.11	3.56
I [12^1-CH_3]	16.49	11.07	8.99	6.18	3.69
K101M					
Heme 1					
B [18^1-CH_3]	29.22	26.67	12.82	4.79	3.36
F [2^1-CH_3]	18.84	17.49	9.55	4.08	2.82
G [12^1-CH_3]	18.01	17.13	8.63	3.57	2.94
Heme 2					
C [18^1-CH_3]	20.36	19.74	16.22	6.43	3.11
D [7^1-CH_3]	20.18	19.22	14.62	5.90	3.13
Heme 3					
E [12^1-CH_3]	19.89	16.64	13.41	13.15	3.47
J [2^1-CH_3]	13.41	13.12	11.21	11.60	4.64
L [7^1-CH_3]	10.21	8.33		8.64	4.00
P [18^1-CH_3]	−3.75	−2.17	−0.82	−0.52	3.65
Heme 4					
A [18^1-CH_3]	30.51	12.65	11.12	7.91	3.24
H [2^1-CH_3]	17.31	8.28	7.48	5.95	3.70
I [12^1-CH_3]	16.43	7.51	7.39	6.13	3.79

S_i denotes the *i*-electron-reduced state.

nals B and F for heme 1, C and D for heme 2, E and P for heme 3, A and H for heme 4, following the selection of signals by ref. 9, and given in Table 3. For wild-type cyt c_3, the average reduction fractions are recalculated using the chemical shifts assigned in ref. 26. The data in Table 3 demonstrate that the order of reduction (major fraction at each step) is hemes 4, 1, 2, and 3, for wild-type, E41K, and K101M cyt c_3.

The microscopic redox potentials of E41K and K101M cyt c_3 at the first and fourth reduction steps (e^I and e^{IV}, respectively, with the subscript representing heme number), and the interacting potentials (I_{ij} for hemes i and j) were determined using the macroscopic redox potentials and the average reduction fractions according to the reported

Table 3 The reduction fractions of the four hemes at the four reduction steps

	R^{I}	R^{II}	R^{III}	R^{IV}
wild type[a]				
Heme 4	0.690	0.063	0.100	0.147
Heme 1	0.080	0.516	0.321	0.083
Heme 2	0.042	0.242	0.522	0.194
Heme 3	0.188	0.179	0.057	0.576
E41K				
Heme 4	0.418	0.181	0.209	0.192
Heme 1	0.286	0.462	0.196	0.057
Heme 2	0.099	0.268	0.482	0.151
Heme 3	0.197	0.089	0.114	0.601
K101M				
Heme 4	0.657	0.059	0.113	0.171
Heme 1	0.089	0.517	0.324	0.070
Heme 2	0.044	0.239	0.537	0.180
Heme 3	0.210	0.185	0.026	0.580

[a] Recalculated from the data reported in ref. 26.

Table 4 The microscopic redox potentials at the first and fourth reduction steps (e_i^{I} and e_i^{IV}, respectively) and the interacting potentials I_{ij}

	Potential/mV (deviation from the wild type)		
	Wild type[a]	E41K	K101M
e_1^{I}	−308	−262 (+46)	−305 (+3)
e_2^{I}	−325	−290 (+35)	−324 (+1)
e_3^{I}	−286	−271 (+15)	−283 (+3)
e_4^{I}	−252	−252 (0)	−253 (−1)
e_1^{IV}	−293	−259 (+34)	−283 (+10)
e_2^{IV}	−315	−285 (+30)	−308 (+7)
e_3^{IV}	−344	−321 (+23)	−339 (+5)
e_4^{IV}	−308	−291 (+17)	−307 (+1)
I_{12}	+30	+12 (−18)	+43 (+13)
I_{13}	−13	−7 (+6)	−20 (−7)
I_{14}	−2	−2 (0)	−1 (+1)
I_{23}	−6	−6 (0)	−5 (+1)
I_{24}	−15	−1 (+14)	−23 (−8)
I_{34}	−39	−36 (+3)	−31 (+8)

Subscripts in *e* and *I* denote heme numbers. The superscripts of *e* show the reduction steps.

[a] Recalculated from the data reported in ref. 26.

method[2,3]. For example, microscopic redox potentials of heme i are given as

$$e_i^{I} = E_I^{\circ\prime} + (TR/F)\ln R_i^{I} \quad (1)$$

$$e_i^{IV} = E_{IV}^{\circ\prime} - (TR/F)\ln R_i^{IV} \quad (2)$$

where T, R and F are absolute temperature, gas constant and Faraday constant, respectively. The results are presented in Table 4 together with the recalculated results for wild-type cyt c_3. The replacement of glutamate by lysine induced large changes in e_1 and e_2. Additionally, certain increases of all e^{IV} were observed, showing that the effect of this mutation was more global in the fourth-reduction step than that in the first-one. On the other hand, the K101M mutation did not induce any significant change in the microscopic redox potentials.

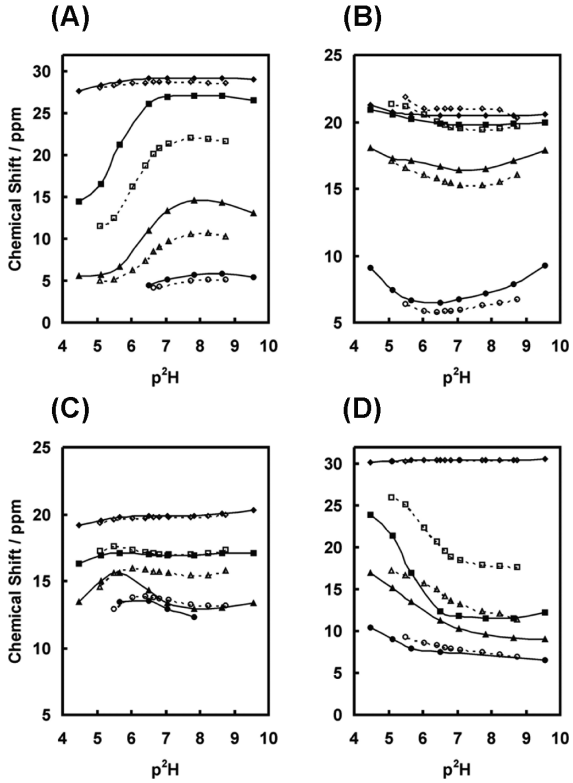

Figure 7 p^2H dependences of the heme methyl signals for wild-type and E41K cytochromes c_3. (A) signal B for heme 1, (B) signal C for heme 2, (C) signal E for heme 3, and (D) signal A for heme 4. Diamonds, squares, triangles, and circles represent the fully oxidized (S_0), one-electron-reduced (S_1), two-electron-reduced (S_2), and three-electron-reduced state (S_3), respectively. Solid lines (closed symbols) and broken ones (open ones) stand for the wild type and E41K, respectively.

p^2H titrations of the heme methyl signals

The p^2H titrations of heme methyl signals in each macroscopic oxidation state were performed for wild type, E41K, and K101M in p^2H ranges of 4.9–9.7, 5.1–8.7, and 5.0–9.5, respectively. The chemical exchange spectra of wild type, E41K, and K101M were recorded at 600 MHz, 600 MHz, and 800 MHz, respectively. The signals in each p^2H were assigned based on the chemical shifts at p^2H 7.0 and previously reported data for wild type[3]. The obtained chemical shifts of the heme methyl signals B (heme 1), C (heme 2), E (heme 3), and A (heme 4) are plotted as a function of p^2H. The titration curves for the wild type and E41K were presented in Figure 7. The titration curves for K101M were similar to those for the wild type. As reported previously, the methyl signals of heme 1 exhibited significant p^2H dependence in the acidic pH region[3]. The midpoints of signal B in the one-electron reduced state determined by the nonlinear least-squares method were 5.6, 6.1, and 5.6 for wild type, E41K, and K101M, respectively. These results indicated that the E41K mutation induced a small shift in the titration curve toward high p^2H. Furthermore, the complicated p^2H dependences were observed in the titration

Table 5 Kinetic parameters of electron transfer between [NiFe] hydrogenase and cytochrome c_3 in 50 mM HEPES buffer at pH 7.0 and 25°C

	K_m/μM	k_{cat}/s^{-1}	$[k_{cat}/K_m]$/μM^{-1} s^{-1}
wild type[a]	2.6±0.3	49±1	19
E41K	2.2±0.3	49±2	23
K101M[a]	9.9±0.9	51±2	5.1

[a] From ref. 18.

curves for heme 3, especially in the two-electron reduced state, which might have something to do with the non-linear change in the chemical shift of the fifth axial ligand of heme 3, His83 (Fig. 1A).

Electron transfer kinetics

To analyze the effect of the E41K mutation on the electron transfer with [NiFe] hydrogenase, the kinetics of the electron transfer was examined. According to the previously described method[18], the steady-state reduction rate of E41K cyt c_3 by hydrogenase was measured. Each rate was plotted as a function of the cyt c_3 concentration and fitted to the Michaelis–Menten equation. Obtained kinetic parameters for E41K are summarized in Table 5. K_m of K101M cyt c_3 is 3.8 times as large as that of wild type as previously reported[18], showing a decrease in the affinity between cyt c_3 and hydrogenase. On the other hand, K_m and k_{cat} of the E41K cyt c_3 were similar to those of the wild type.

Crystal structures of E41K and E41Q cytochromes c_3

The refinements of the crystal structures for the oxidized E41K (PDB code 1WR5) and E41Q (PDB code 2FFN) cyt c_3 have been completed at 1.40 and 1.80 Å resolution, respectively. The crystallographic R- (free R-) factors of E41K and E41Q are 13.83 (21.83) and 17.04 (21.66) %, respectively. 17 ethanol molecules were identified in the E41K structure. The overall structures of E41K and E41Q cyt c_3 were almost identical to that of the wild type[20], as shown in Figure 8. The root mean square deviations (rmsd) of E41K and E41Q with respect to the wild type for all identical atoms in the residue range from K3 to C105 and four hemes were 0.58 and 0.53 Å, respectively. In the crystal structure of E41K, a hydrogen bond was formed between O^{η} atom of Tyr43 and N^{ζ} atom of Lys41 (3.30 Å). The conformation of Gln41 in E41Q was similar to Glu41 in the wild type ($O^{\varepsilon 1}$(Gln41) – O^{η}(Tyr43) = 2.82 Å, $O^{\varepsilon 1}$(Glu41) – O^{η}(Tyr43) = 2.75 Å, Fig. 8B).

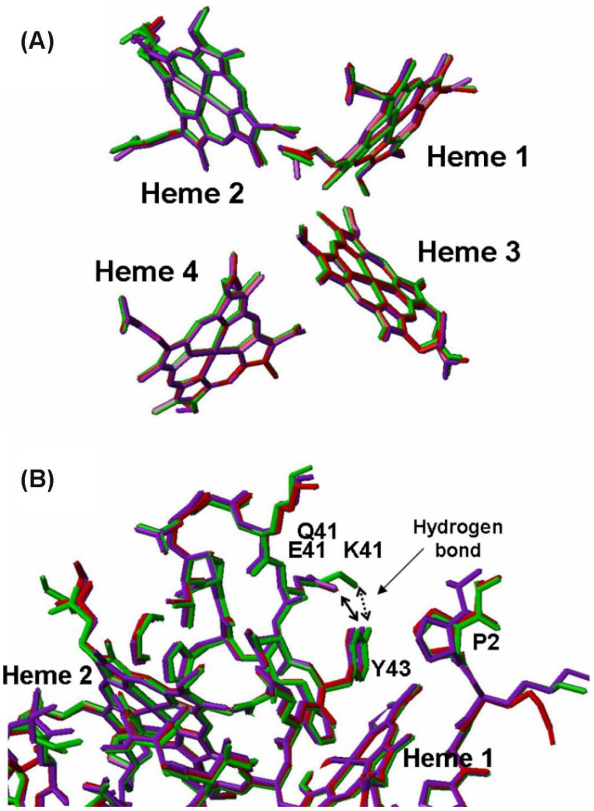

Figure 8 Comparison of the crystal structures of wild-type, E41K, and E41Q cytochromes c_3. The four heme architecture (A) and the region between hemes 1 and 2 (B) of the wild type, E41K, and E41Q under the best fitting for the Cα of K3–C105 residues. The structure models are color-coded red, green, and purple for the wild type, E41K, and E41Q, respectively. These figures were drawn with MOLMOL[38].

Discussion

In the pH titrations of ^1H-^{15}N HSQC spectra, the NH signal of Cys46 revealed the largest shift in the oxidized and reduced states (Figs. 1B and 2B), and in the pK_a (Fig. 4C). The amide proton of Cys46 forms a hydrogen bond with the carboxyl oxygen of heme 1 C13-propionate in the oxidized crystal structure[19]. The protonation of this propionate group would directly affect the NH signal of Cys46 in the oxidized state. On the other hand, the conformational change of the region between hemes 1 and 2 takes place in the reduced state, so that the propionate at C13 of heme 1 is located close to Leu9, Lys10, and Lys45 (Fig. 3B)[17]. The NH signals of these three residues revealed larger transitions in the reduced state than those in the oxidized one (Fig. 4C). Furthermore, these behaviors are similar to that of Cys46. Consequently, these pH-dependent behaviors for Leu9, Lys10, Lys45, and Cys46 must be caused by the protonation of the propionate at C13 of heme 1. On the other hand, the NH signals for the Glu41 and Asp42 revealed the same behavior in the oxidized and reduced states (Fig. 4A), which demonstrated that these residues were not affected by the C13 propionate of heme 1 directly. Namely, chemical shift changes of the NH signals for Glu41 and Asp42 were caused by the protonation of carboxyl group in each residue.

In the basic pH region, the residues around heme 2 indicated the larger chemical shift changes in both redox states (Fig. 3). Among these residues, His67 is the only one with a pK_a between pH 7 and 9 in the theoretical calculations for *Dv*MF cyt c_3[13]. Glu41, Asp42 and propionate groups of

hemes cannot contribute to the pH dependence in the basic region in view of their low pK_a. Therefore, these large NH signal transitions from pH 7 to 9 should be mainly caused by the protonation of His67 imidazole group. Furthermore, the transitions of heme 2 methyl signals in the basic pH region (Fig. 7B) should be mainly ascribed to His67, too. A previous report indicated that the interacting potential between hemes 1 and 2 (I_{12}) at p^{2}H 9.0 is smaller than that at p^{2}H 7.1[3]. This deprotonation may induce a small decrease in the positive cooperativity between hemes 1 and 2. As reported previously, H67A and H67Q mutations did not influence the redox potentials at pH 7.0[9], but it may play a certain role in the basic pH region.

The Glu41 mutations showed large changes in the redox potentials at pH 7.0 (Tables 1 and 4). This is consistent with the previous report that the contributions of Glu41 to the electrostatic potential at heme irons of hemes 1 and 2 are relatively high[34]. On the other hand, the mutations of lysines 10, 15, 26, 57, 58, 60, 72, 94, 95, and 104 to methionine did not induce large changes in the macroscopic redox potentials[18]. In the case of the K101M mutant, the microscopic as well as the macroscopic redox potentials were the same as those of the wild type. The crystal structure of E41K showed a slight alteration of Tyr43 because of the hydrogen bond between Lys41 and Tyr43 (Fig. 8B). This alteration may change the strength of the π-π interaction between the aromatic ring of Tyr43 and the imidazole ring of His34, so that the microscopic redox potentials might increase. A strong coordination of His34 to Fe^{3+} would induce a slight polarization in the electron density of imidazole ring, which can be stabilized by π electron density of the Tyr43 ring through the π-π interaction. Thus, a redox potential would be lowered by the π-π interaction. A careful examination of the eight signals of the axial ligand histidine C2 protons in the ^{1}H NMR spectra of the E41K, Y43L[20], and E41Q mutants (Fig. 9) revealed significant shifts for the signal marked by asterisk in comparison with the wild type, supporting the idea that those mutations affect the coordination structure of a heme ligand. This signal could be assigned to the His34 because it is the closest histidine ligand to the Glu41 and Tyr43 residues. It should be noted that the crystal structures did not have enough resolution to show this kind of change in the coordination structure.

In the p^{2}H titration curves of heme methyl signals (Fig. 7), the chemical shift changes depending on the redox stages caused by E41K mutation were very large, but the pK_a shift is small compared with Lys45 mutations for *Dv*H cyt c_3[11]. This is reasonable because the pK_a shift of the NH signal for Glu41 is redox-independent (Fig. 4A) and the propionate at C13 of heme 1 is not directly affected by the E41K mutation in the crystal structure (Fig. 8A). It has been reported that the heme methyl signals of heme 3 behaves unusually during the process of reduction[26]. In this study, this unusual property of heme 3 was observed as the pH dependences of the heme methyl signal (Fig. 7C) and the

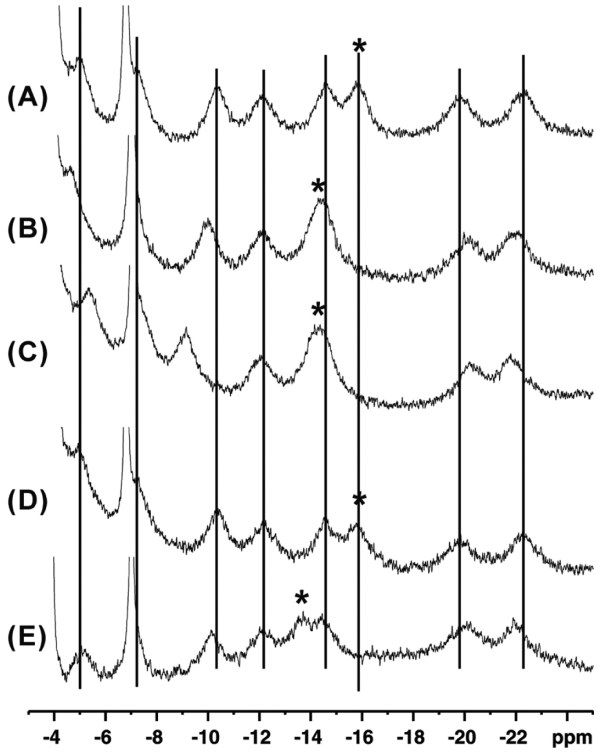

Figure 9 ^{1}H NMR spectra of axial ligand histidine C2 proton for wild-type and mutated ferric cytochromes c_3 at 303 K. (A) wild type, (B) E41K, (C) Y43L[20], (D) wild type, and (E) E41Q, respectively. (A–C) and (D, E) are recorded in 30 and 100 mM sodium phosphate buffers at p^{2}H 7.0, respectively. Asterisks indicate the signals which could be assigned to His34.

NH signal for His83 (Fig. 1A). Furthermore, the signal J of heme 3 for E41K cyt c_3 indicated different behavior from that of wild type (Table 2), which indicated this mutation affected the intermediate oxidation states. Consequently, small pK_a shift for E41K cyt c_3 would be induced by the change of the environment around the propionate at C13 of heme 1, including heme 3. Based on this work, the p^{2}H titration curves in Figure 7 have confirmed that they are not as simple as indicated by A. V. Xavier and his colleagues, who have analyzed all their data for *Dv*H cyt c_3 as well as our *Dv*MF cyt c_3, assuming just one transition on a pH titration curve at every oxidation state[4,5,11]. An introduction of single pK_a in the thermodynamic analysis is an oversimplified model.

Additionally, in the electron transfer with [NiFe] hydrogenase, the E41K mutation did not affect K_m, which indicates Glu41 is not involved in the complex formation with hydrogenase. k_{cat}, which reflects the electron transfer rate, was not affected by this mutation, too. If the heme 1 also serves as the gate to accept electrons, k_{cat} might be increased because the driving force of heme 1 in E41K cyt c_3 is increased by up to 46 mV compared to that of wild type. Namely, heme 1 (e_1^1=−262 mV) of E41K can accept electron from the distal [4Fe4S] cluster (about −290 mV)[35,36] of

hydrogenase simply from the view point of driving force. On top of it, the microscopic redox potential, e_4^I, of E41K was the same as that of the wild type. These results support the conclusion that the region around heme 4 forms complex with [NiFe] hydrogenase and the heme 4 works as the exclusive entrance gate of electrons in the initial reduction[18].

In summery, the redox-linked pK_a shifts of heme methyl signals (Fig. 7) are caused by the propionate group at C13 of heme 1, which is consistent with the redox-linked conformational change. This pK_a shift is important to the cooperative reduction between hemes 1 and 2. And then, Glu41 is significant to maintain the internal region containing Tyr43 and His34 which is controlling the redox properties of four hemes although it is not involved in the interaction with [NiFe] hydrogenase. Furthermore, the deprotonation of His67, which was noticed in the theoretical studies[15], was experimentally observed for the first time. These charged residues generate the pH-dependent redox properties of four hemes around the neutral pH range. It is expected the further examination of these charged residues which complicate the redox property of *Dv*MF cyt c_3.

Acknowledgement

We are grateful to Prof. Takahisa Ikegami (Osaka University) for assistance in the NMR facility and Dr. Yuki Takayama (Osaka University) for his fruitful discussion.

References

1. Marcus, R. A. & Sutin, N. Electron transfers in chemistry and biology. *Biochim. Biophys. Acta* **811**, 265–322 (1985).
2. Fan, K., Akutsu, H., Kyogoku, Y. & Niki, K. Estimation of microscopic redox potentials of a tetraheme protein, cytochrome c_3 of *Desulfovibrio vulgaris*, Miyazaki F, and partial assignments of heme groups. *Biochemistry* **29**, 2257–2263 (1990).
3. Park, J.-S., Ohmura, T., Kano, K., Sagara, T., Niki, K., Kyogoku, Y. & Akutsu, H. Regulation of the redox order of four hemes by pH in cytochrome c_3 from *D. vulgaris* Miyazaki F. *Biochim. Biophys. Acta* **1293**, 45–54 (1996).
4. Turner, D. L., Salguerio, C. A., Catarino, T., LeGall, J. & Xavier, A. V. Homotropic and heterotropic cooperativity in the tetrahaem cytochrome c_3 from *Desulfivibrio vulgaris*. *Biochim. Biophys. Acta* **1187**, 232–235 (1994).
5. Turner, D. L., Salguerio, C. A., Catarino, T., LeGall, J. & Xavier, A. V. NMR studies of cooperativity in the tetrahaem cytochrome c_3 from *Desulfovibrio vulgaris*. *Eur. J. Biochem.* **241**, 723–731 (1996).
6. Louro, R. O., Catarino, T., LeGall, J., Turner, D. L. & Xavier, A. V. Cooperativity between electrons and protons in a monomeric cytochrome c_3: the importance of mechano-chemical coupling for energy transduction. *CHEMBIOCHEM* **2**, 831–837 (2001).
7. Coletta, M., Catarino, T., LeGall, J. & Xavier, A. V. A thermodynamic model for the cooperative functional properties of the tetraheme cytochrome c_3 from *Desulfovibrio gigas*. *Eur. J. Biochem.* **202**, 1101–1106 (1991).
8. Louro, R. O., Catarino, T., Turner, D. L., Piçarra-Pereira, M. A., Pacheco, I., LeGall, J. & Xavier, A. V. Functional and mechanistic studies of cytochrome c_3 from *Desulfovibrio gigas*: thermodynamics of a "proton thruster". *Biochemistry* **37**, 15808–15815 (1998).
9. Takayama, Y., Harada, E., Kobayashi, R., Ozawa, K. & Akutsu, H. Roles of noncoordinated aromatic residues in redox regulation of cytochrome c_3 from *Desulfovibrio vulgaris* Miyazaki F. *Biochemistry* **43**, 10859–10866 (2004).
10. Bento, I., Matias, P. M., Baptista, A. M., da Costa, P. N., van Dongen, W. M. A. M., Saraiva, L. M., Schneider, T. R., Soares, C. M. & Carrondo, M. A. Molecular basis for redox-Bohr and cooperative effects in cytochrome c_3 from *Desulfovibrio desulfuricans* ATCC 27774: crystallographic and modeling studies of oxidized and reduced high-resolution structures at pH 7.6. *Proteins* **54**, 135–152 (2004).
11. Saraiva, L. M., Salgueiro, C. A., da Costa, P. N., Messias, A. C., LeGall, J., van Dongen, W. M. A. M. & Xavier, A. V. Replacement of lysine 45 by uncharged residues modulates the redox-Bohr effect in tetraheme cytochrome c_3 of *Desulfovibrio vulgaris* (Hildenborough). *Biochemistry* **37**, 12160–12165 (1998).
12. Soares, C. M., Martel, P. J. & Carrondo, M. A. Theoretical studies on the redox-Bohr effect in cytochrome c_3 from *Desulfovibrio vulgaris* Hildenborough. *J. Biol. Inorg. Chem.* **2**, 714–727 (1997).
13. Martel, P. J., Soares, C. M., Baptista, A. M., Fuxreiter, M., Náray-Szabó, G., Louro, R. O. & Carrondo, M. A. Comparative redox and pK_a calculations on cytochrome c_3 from several *Desulfovibrio* species using continuum electrostatic methods. *J. Biol. Inorg. Chem.* **4**, 73–86 (1999).
14. Baptista, A. M., Martel, P. J. & Soares, C. M. Simulation of electron-proton coupling with a Monte Carlo method: application to cytochrome c_3 using continuum electrostatics. *Biophys. J.* **76**, 2978–2998 (1999).
15. Teixeira, V. H., Soares, C. M. & Baptista, A. M. Studies of the reduction and protonation behavior of tetraheme cytochromes using atomic detail. *J. Biol. Inorg. Chem.* **7**, 200–216 (2002).
16. Oliveira, A. S. F., Teixeira, V. H., Baptista, A. M. & Soares, C. M. Reorganization and conformational changes in the reduction of tetraheme cytochromes. *Biophys. J.* **89**, 3919–3930 (2005).
17. Harada, E., Fukuoka, Y., Ohmura, T., Fukunishi, A., Kawai, G., Fujiwara, T. & Akutsu, H. Redox-coupled conformational alternations in cytochrome c_3 from *D. vulgaris* Miyazaki F on the basis of its reduced solution structure. *J. Mol. Biol.* **319**, 767–778 (2002).
18. Yahata, N., Saitoh, T., Takayama, Y., Ozawa, K., Ogata, H., Higuchi, Y. & Akutsu, H. Redox interaction of cytochrome c_3 with [NiFe] hydrogenase from *Desulfivibrio vulgaris* Miyazaki F. *Biochemistry* **45**, 1653–1662 (2006).
19. Higuchi, Y., Kusunoki, M., Matsuura, Y., Yasuoka, N. & Kakudo, M. Refined structure of cytochrome c_3 at 1.8 Å resolution. *J. Mol. Biol.* **172**, 109–139 (1984).
20. Ozawa, K., Takayama, Y., Yasukawa, F., Ohmura, T., Cusanovich, M. A., Tomimoto, Y., Ogata, H., Higuchi, Y. & Akutsu, H. Role of the aromatic ring of Tyr43 in tetraheme cytochrome c_3 from *Desulfovibrio vulgaris* Miyazaki F. *Biophys. J.* **85**, 3367–3374 (2003).
21. Teixeira, V. H., Baptista, A. M. & Soares, C. M. Modeling electron transfer thermodynamics in protein complexes: interaction between two cytochromes c_3. *Biophys. J.* **86**, 2773–2785 (2004).
22. Pieulle, L., Morelli, X., Gallice, P., Lojou, E., Barbier, P., Czjzek, M., Bianco, P., Guerlesquin, F. & Hatchikian, E. C. The type I/type II cytochrome c_3 complex: an electron trans-

fer link in the hydrogen-sulfate reduction pathway. *J. Mol. Biol.* **354**, 73–90 (2005).
23. Matias, P. M., Soares, C. M., Saraiva, L. M., Coelho, R., Morais, J., LeGall, J. & Carrondo, M. A. [NiFe] hydrogenase from *Desulfovibrio desulfuricans* ATCC 27774: gene sequencing, three-dimensional structure determination and refinement at 1.8 Å and modeling studies of its interaction with the tetraheme cytochrome c_3. *J. Biol. Inorg. Chem.* **6**, 63–81 (2001).
24. Ozawa, K., Yasukawa, F., Fujiwara, Y. & Akutsu, H. A Simple, rapid, and highly efficient gene expression system for multiheme cytochromes *c*. *Biosci. Biotechnol. Biochem* **65**, 185–189 (2001).
25. Park, J.-S., Kano, K., Niki, K. & Akutsu, H. Full assignment of heme redox potentials of cytochrome c_3 of *D. vulgaris* Miyazaki F by ^{1}H-NMR. *FEBS Lett.* **285**, 149–151 (1991).
26. Ohmura, T., Inobe, T., Kano, K., Horizumi, T. & Akutsu, H. Unusual behavior of a heme in a tetraheme protein, cytochrome c_3 from *Desulfivibrio vulgaris* Miyazaki F, in the reduction process. *J. Electroanal. Chem.* **438**, 237–243 (1997).
27. Niki, K., Kobayashi, Y. & Matsuda, H. Determination of macroscopic standard potentials of a molecule with a reversible *n*-consecutive one-electron-transfer process. Application to a tetraheme protein: cytochrome c_3. *J. Electroanal. Chem.* **178**, 333–341 (1984).
28. Leslie, A. G. W. MOSFILM Version 5.41; MRC Laboratory of Molecular Biology. (Oxford University Press, Cambridge, UK, 1994).
29. Collaborative Computational Project, Number 4, SERC Daresbury Laboratory. The *CCP*4 suite: programs for protein crystallography. *Acta Crystallogr.* **D50**, 760–763 (1994).
30. Brünger, A. T., Adams, P. D., Clore, G. M., DeLano, W. L., Gros, P., Grosse-Kunstleve, R. W., Jiang, J.-S., Kuszewski, J., Nilges, M., Pannu, N. S., Read, R. J., Rice, L. M., Simonson, T. & Warren, G. L. Crystallography & NMR system: a new software suite for macromolecular structure determination. *Acta Crystallogr.* **D54**, 905–921 (1998).
31. Sheldrick, G. M. & Schneider, T. R. SHELXL: High-resolution refinement. *Methods Enzymol.* **277**, 319–343 (1997).
32. Wishart, D. S., Sykes, B. D. & Richards, F. M. Relationship between nuclear magnetic resonance chemical shift and protein secondary structure. *J. Mol. Biol.* **222**, 311–333 (1991).
33. Ozawa, K., Tsapin, A. I., Nealson, K. H., Cusanovich, M. A. & Akutsu, H. Expression of a tetraheme protein, *Desulfivibrio vulgaris* Miyazaki F cytochrome c_3, in *Shewanella oneidensis* MR-1. *Appl. Environ. Microbiol.* **66**, 4168–4171 (2000).
34. Ohmura, T., Nakamura, H., Niki, K., Cusanovich, M. A. & Akutsu, H. Ionic strength-dependent physicochemical factors in cytochrome c_3 regulating the electron transfer rate. *Biophys. J.* **75**, 1483–1490 (1998).
35. Teixeira, M., Moura, I., Xavier, A. V., Moura, J. J. G., LeGall, J., DerVartanian, D. V., Peck, Jr., H. D. & Huynh, B.-H. Redox intermediates of *Desulfovibrio gigas* [NiFe] hydrogenase generated under hydrogen. Mössbauer and EPR characterization of the metal centers. *J. Biol. Chem.* **264**, 16435–16450 (1989).
36. Asso, M., Guigliarelli, B., Yagi, T. & Bertrand, P. EPR and redox properties of *Desulfovibrio vulgaris* Miyazaki hydrogenase: comparison with the Ni-Fe enzyme from *Desulfovibrio gigas*. *Biochim. Biophys. Acta* **1122**, 50–56 (1992).
37. Pettersen, E. F., Goddard, T. D., Huang, C. C., Couch, G. S., Greenblatt, D. M., Meng, E. C. & Ferrin, T. E. UCSF Chimera — a visualization system for exploratory research and analysis. *J. Comput. Chem.* **25**, 1605–1612 (2004).
38. Koradi, R., Billeter, M. & Wüthrich, K. MOLMOL: a program for display and analysis of macromolecular structures. *J. Mol. Graphics* **14**, 51–55 (1996).